A vibrational spectroscopic study of hydrated Fe^{3+} hydroxyl-sulphates; polymorphic minerals butlerite and parabutlerite

Jiří Čejka, [1,2] Jiří Sejkora,[2.] Jakub Plášil, [2] Silmarilly Bahfenne, [1] Sara J. Palmer,[1] Llew Rintoul and Ray L. Frost [1] •

[1] Chemistry Discipline, Faculty of Science and Technology, Queensland University of Technology, GPO Box 2434, Brisbane Queensland 4001, Australia.

[2] National Museum, Václavské náměstí 68, CZ-115 79 Praha 1, Czech Republic.

ABSTRACT

Raman and infrared spectra of two polymorphous minerals with the chemical formula $Fe^{3+}(SO_4)(OH)\cdot 2H_2O$, monoclinic butlerite and orthorhombic parabutlerite, are studied and the spectra assigned. Observed bands are attributed to the $(SO_4)^{2-}$ stretching and bending vibrations, hydrogen bonded water molecules, stretching and bending vibrations of hydroxyl ions, water librational modes, Fe-O and Fe-OH stretching vibrations, Fe-OH bending vibrations and lattice vibrations. The O-H...O hydrogen bond lengths in the structures of both minerals are calculated from the wavenumbers of the stretching vibrations. One symmetrically distinct $(SO_4)^{2-}$ unit in the structure of butlerite and two symmetrically distinct $(SO_4)^{2-}$ units in the structure of parabutlerite are inferred from the Raman and infrared spectra. This conclusion agrees with the published crystal structures of both mineral phases.

Keywords: butlerite, parabutlerite, iron(III) sulphates, Raman spectroscopy, infrared spectroscopy, hydroxyl ions, molecular water, hydrogen bonds

• Author to whom correspondence should be addressed (r.frost@qut.edu.au)

INTRODUCTION

The Fe^{2+} and Fe^{3+} sulfates are the main products of weathering of iron sulphides and Fe-containing alloys under oxidation conditions with different activity of sulfate ions and pH values [1]. Recently, the sulphates of iron were observed on the Mars surface [2] and their abundant occurrences are found in some evaporite deposits [3-4], especially when found in an arid environment.

Butlerite [5,6] and parabutlerite [5,7] are two dimorphous hydrated ferric hydroxyl-sulfate minerals of formula $Fe^{3+}(SO_4)(OH)\cdot 2H_2O$. Butlerite is monoclinic, *a* 6.44-6.50, *b* 7.31-7.38, *c* 5.84-5.87 Å, β 108°23(5)'- 108°28(20)' with space group $P2_1/m$, Z = 2, while parabutlerite is orthorhombic, *a* 7.38, *b* 20.13, *c* 7.22 with space group *Pmnb*, Z = 8 [5-11]. The minerals are formed in the oxidation zones of pyrite ores but may also be formed under fumarolic conditions such as with volcanos and mine fires [12]. No doubt, the minerals are involved in paragenetic relationships with other ferrous and ferric sulphates. Bandy [13] in his classic description of the sulfate deposits of Chile described sequences of the ferric and ferrous/ferric sulfate minerals at these mine sites. A number of factors including temperature, relative humidity, sulphuric acid concentration and the presence of other cations determine which ferrous or ferric sulfate mineral is formed.

Williams [4] described the complex phase equilibria involving SO_3, Fe_2O_3 and H_2O. He showed there is a specific phase region in which monoclinic butlerite is found in the triangular phase diagram for the system Fe_2O_3-H_2O-SO_3 at 50 °C. The crystal structure of butlerite was solved by Fanfani et al. [6], while that of parabutlerite was determined by Borène [7]. According to Hawthorne et al. [14-17], the $[M(S\phi_4)\phi_3]$ chain is the basis of crystal structure of butlerite, $[Fe^{3+}(OH)(H_2O)_2(SO_4)]$, and parabutlerite, $[Fe^{3+}(OH)(H_2O)_2(SO_4)]$, where $\phi = (OH)^-, (O)^{2-}, H_2O$. In this chain, the $(SO_4)^{2-}$ tetrahedra alternate along the chain and link to trans vertices of the $(Fe^{3+}\phi_6)$ octahedra. In butlerite and parabutlerite, the $[Fe^{3+}(OH)(H_2O)_2(SO_4)]$ chains are linked solely by hydrogen bonds. No interstitial cations are present in the structure. The chains in butlerite and parabutlerite structures are extremely similar. The principal structural difference is in the relative disposition of adjacent chains [14]. In the crystal structure of butlerite there is one crystallographically distinct Fe^{3+} and one crystallographically distinct S^{6+} [6]. One unique

Fe^{3+} site and two crystallographically distinct S^{6+} sites were found in the crystal structure of parabutlerite [7]. In both crystal structures, the Fe^{3+} octahedra ($Fe^{3+}\phi_6$) contain two $(O)^{2-}$, two $(OH)^{-}$ and two water molecules, which are coordinated by oxygens to the cations [6,7]. $[Fe(OH)(H_2O)_2SO_4]$ spiral chains observed in the structure of fibroferrite are a stereoisomer variant of the hydroxo-bridged linear chains in the structure of butlerite and parabutlerite [18]. Only Raman spectrum of parabutlerite is available in the RRUFF database (parabutlerite R070547) but without any details of wavenumbers and interpretation.

As part of our on-going research into supergene mineral formation [19-20], this paper reports the Raman spectra of butlerite and parabutlerite and relates the spectra to the molecular structure of both sulfate minerals studied [21-22].

EXPERIMENTAL

Minerals

The mineral samples of butlerite and parabutlerite were obtained from the mineralogical collections of the National Museum Prague, Czech Republic. Both minerals originated from the Alcaparrosa mine, Cerritos Bayos, Calama, El Loa Province, Antofagasta, Chile. Butlerite is light yellow with fine-grained aggregates (some cm in size), and were found in association with anhydrite, copiapite and botryogen. Parabutlerite forms pale orange prismatic crystals, up to some mm in size, in cavities of sulfate (copiapite, botryogen and anhydrite) matrixes. Both minerals were analysed for phase purity by X-ray powder diffraction, and no significant impurities were found. The measured X-ray powder diffraction patterns of both minerals agree very well with the published data. The refined unit-cell parameters for butlerite are: *a* 6.527(2), *b* 7.376(1), *c* 5.860(2) Å, β 108.57(1)^{o} and *V* 267.4(1) Å^3 (monoclinic space group $P2_1/m$), which agrees very well with parameters from single-crystal measurements [6]. The refined unit-cell parameters for parabutlerite are: *a* 7.398(2), *b* 20.170(4), *c* 7.230(1) Å, *V* 1073.5(5) Å^3 (orthorhombic space group *Pmnb*), which also agrees well with parameters from single-crystal measurements [7].

Both samples were quantitatively analysed by Cameca SX 100 microprobe system in wavelength dispersion mode for chemical composition. The samples were mounted onto the epoxide resin and polished. The polished surface was coated with a carbon layer of 250 Å. An acceleration voltage of 15 kV, a specimen current of 10 nA, a beam diameter of 10 μm and a suite of well-defined natural and synthetic standards were used. The raw intensities were converted to the concentrations using the automatic *PAP* matrix correction software package. The H_2O content was calculated from charge balance and theoretical contents of water molecules. The chemical composition of butlerite was Fe_2O_3 38.96, Al_2O_3 0.04, SiO_2 0.18, SO_3 36.88, $H_2O_{calc.}$ 21.51, sum 97.57 wt. % and empirical formula on the basis 1 (S+Si) *apfu* is $Fe^{3+}_{1.05}[(SO_4)_{0.99}(SiO_4)_{0.01}]_{\Sigma 1.00}(OH)_{1.15}\cdot 2H_2O$ (mean of 4 point analyses). The chemical composition of parabutlerite was Fe_2O_3 39.42, Al_2O_3 0.05, SiO_2 0.05, SO_3 37.24, $H_2O_{calc.}$ 21.75, sum 98.52 wt. % and empirical formula on the basis 1 (S+Si) *apfu* is $Fe^{3+}_{1.06}(SO_4)_{1.00}(OH)_{1.18}\cdot 2H_2O$ (mean of 6 point analyses).

Raman and infrared spectroscopy

Crystals of butlerite and parabutlerite were placed on a polished metal surface on the stage of an Olympus BHSM microscope, which is equipped with 10x, 20x, and 50x objectives. The microscope is part of a Renishaw 1000 Raman microscope system, which also includes a monochromator, a filter system and a CCD detector (1024 pixels). The Raman spectra were excited by a Spectra-Physics model 127 He-Ne laser producing highly polarised light at 633 nm and collected at a nominal resolution of 2 cm^{-1} and a precision of ± 1 cm^{-1} in the range between 200 and 4000 cm^{-1}. Repeated acquisition on the crystals using the highest magnification (50x) were accumulated to improve the signal to noise ratio of the spectra. Spectra were calibrated using the 520.5 cm^{-1} line of a silicon wafer. Previous studies by the authors provide more details of the experimental technique. Alignment of all crystals in a similar orientation has been attempted and achieved. However, differences in intensity may be observed due to minor differences in the crystal orientation.

Infrared spectra were obtained using a Nicolet 6700 FTIR spectrometer with a single bounce diamond GladATR (PIKE) cell. Spectra over the 4000–400 cm^{-1} range were obtained by the co-addition of 128 scans with a resolution of 4 cm^{-1} and a mirror velocity of 0.63 cm/s. Spectra were co-added to improve the signal to noise ratio.

Spectral manipulation such as baseline correction/adjustment and smoothing were performed using the Spectracalc software package GRAMS (Galactic Industries Corporation, NH, USA). Band component analysis was undertaken using the Jandel 'Peakfit' software package that enabled the type of fitting function to be selected and allows specific parameters to be fixed or varied accordingly. Band fitting was done using a Lorentzian-Gaussian cross-product function with the minimum number of component bands used for the fitting process. The Gaussian-Lorentzian ratio was maintained at values greater than 0.7 and fitting was undertaken until reproducible results were obtained with squared correlations of r^2 greater than 0.995.

RESULTS AND DISCUSSION

Spectroscopy background

Free sulfate, $(SO_4)^{2-}$, of *T*d symmetry, exhibits four fundamental vibrations: the ν_1 (A_1) symmetric stretching vibration – Raman active, the ν_2 (E) doubly degenerate symmetric bending vibration – Raman active, the ν_3 (F_2) triply degenerate antisymmetric stretching vibration – infrared and Raman active, and the ν_4 (F_2) triply degenerate antisymmetric bending vibration – infrared and Raman active [23-25]. According to Myneni [23], variation in salvation (coordination of water molecules at different oxygen atoms of sulfate ion), metal complexation, and protonation of sulfate can modify the S-O bond lengths, and cause changes in symmetry from T_d to either C_{3v}/C_3 (monodentate, corner-sharing), C_{2v}/C_2 (edge-sharing, bidentate binuclear), or C_1/C_s (corner-sharing, edge-sharing, bidentate binuclear, multidentate). Myneni writes that such changes may shift the vibrational bands to different energies and cause the degenerate vibrations to become nondegenerate [23]. In dilute aqueous solutions of pH > 3.0, $(SO_4)^{2-}$ occurs primarily as a tetrahedral species and exhibits corresponding stretching and bending vibrations at 983, 450, 1105 and 611 cm^{-1} [23,24].

Factor group analysis of the sulfate for the sites and crystal symmetries found in bultlerite and parabutlerite, respectively, is summarised in Table 1. The sulfate symmetric stretch in butlerite is expected to give rise to one Raman active band and one IR active band, whereas two Raman and two IR bands are predicted for each of the 2 unique sulfates in

parabutlerite to give a total of 4 Raman and 4 IR bands. The triply degenerate modes such as the antisymmetric stretch and deformation of sulfate lose their degeneracy owing to the Cs site symmetry in both minerals. Crystal splitting leads to mutual exclusion between the IR and Raman and thus 3 Raman and 3 IR bands are expected for butlerite. With 2 unique sulfate groups, the situation is somewhat complicated in parabutlerite where a total of 12 Raman bands and 12 IR bands are expected for the antisymmetric F_2 modes.

The $(OH)^-$ ions display stretching, bending, librational (restricted rotation) and translational vibrations. The OH stretching modes range from 3700 to 3550 cm^{-1} in the case of hydroxyls, which are not involve in hydrogen bonds, and 3570 to 3200 cm^{-1} for hydroxyls involved in hydrogen bonding. The OH bending vibrations are located up to approximately 1700 cm^{-1} and over a wide range below this value. The OH librational modes are observed from 1000 to 300 cm^{-1} and lattice vibrations involving $(OH)^-$ ion motions are found from 400 to 150 cm^{-1} [25,26]. Molecular water is characterized by three fundamentals, the ν_1 (A_1) symmetric stretching vibration and the ν_3 (B_1) antisymmetric stretching vibration, both in the range of 3600 to 2900 cm^{-1}, and the ν_2 (δ) (A_1) bending vibration, located approximately from 1590 to 1700 cm^{-1}. Some shifting of the stretching vibrations to lower wavenumbers and the bending vibrations to higher wavenumbers are observed when water molecules are involved in stronger hydrogen bonding. In this case, libration modes can occur approximately in the range from 900 to 300 cm^{-1}. All stretching and bending vibrations are infrared and Raman active [25]. Factor group analysis of the $(OH)^-$ ions predicts 2 Raman bands and 2 IR bands for each of the OH stretch and OH libration in parabutlerite (4 Raman and 4 IR bands in total) but only 1 Raman and 1 IR band for butlerite.

The Raman spectra of butlerite and parabutlerite are displayed in Figs. 1a and 1b, respectively, while Table 2 gives a summary of band positions and assignments. The Raman spectrum of butlerite in the 900 to 1300 cm^{-1} region shows an intense Raman band at 1024 cm^{-1} assigned to the ν_1 $(SO_4)^{2-}$ symmetric stretching mode. The band shows some asymmetry on the low wavenumber side. Band fitting results reveal weak bands at 1014, 1036 and a very weak peak at 983 cm^{-1}, yet factor group analysis predicts only one band for the symmetric sulfate stretch. In contrast, in the Raman spectrum of parabutlerite, two Raman bands are found at 1014 and 1026 cm^{-1} and are attributed to ν_1 $(SO_4)^{2-}$ symmetric stretching modes. Both bands are strong and very sharp. The observation of two bands provides further

194 evidence for the non-equivalence of the sulfate units in the parabutlerite structure. Other
195 bands are observed at 1044 and 990 cm^{-1}. Factor group analysis predicts that the two unique
196 SO_4^{-2} groups gives rise to 2 bands in the symmetric stretching region, in apparent agreement
197 with the number observed. However, in the case of butlerite and parabutlerite, some of bands
198 in this region may be in fact related to the Fe-OH bending vibrations. This would account for
199 one of the additional bands observed in the butlerite spectrum. It should be noted that the
200 sharp strong band of parabutlerite at 1014 cm^{-1}corresponds to one of the additional bands in
201 butlerite .
202
203 In butlerite Raman bands are also found at 1088, 1109, 1145, 1198 and 1225 cm^{-1} and
204 are attributed to the split triply degenerate ν_3 $(SO_4)^{2-}$ antisymmetric stretching mode. Factor
205 group analysis only predicts 3 bands in this region. In contrast, in the Raman spectrum of
206 parabutlerite, four Raman bands are observed at 1095, 1109, 1164 and 1202 cm^{-1}. These
207 bands are also assigned to the split triply degenerate ν_3 $(SO_4)^{2-}$ antisymmetric stretching
208 vibrations. The presence of one symmetrically distinct $(SO_4)^{2-}$ unit in the structure of butlerite
209 and two symmetrically distinct $(SO_4)^{2-}$ units in the structure of parabutlerite, inferred from the
210 Raman spectra, is in agreement with the X-ray single crystal structures of butlerite [6] and
211 parabutlerite [7].
212
213 The infrared spectra of butlerite and parabutlerite in the 1300 to 700 cm^{-1} region are
214 displayed in Figs. 2a and 2b. The spectra show considerable band overlap. However,
215 through band component analysis, component bands may be resolved (Table 3). Infrared
216 bands and shoulders are observed for butlerite at 950, 998, 1050, 1099, 1175 and 1225 cm^{-1}.
217 Infrared bands and shoulders are observed for parabutlerite at 956, 994, 1051, 1097, 1131,
218 1173 and 1228 cm^{-1}. The infrared band at 998 cm^{-1} for butlerite and at 994 cm^{-1} for
219 parabutlerite are attributed to the $(SO_4)^{2-}$ ν_1 symmetric stretching mode. The infrared bands of
220 butlerite at 1050, 1099, 1175 and 1225 cm^{-1} and at 1051, 1097, 1131, 1173 and 1228 cm^{-1} for
221 parabutlerite are assigned to the split triply degenerate ν_3 $(SO_4)^{2-}$ antisymmetric stretching
222 vibrations. The infrared shoulders at 950 cm^{-1} for butlerite and at 956 cm^{-1} for parabutlerite
223 are assigned to the Fe-OH bending vibrations, which appeared as a shoulder at 990 cm^{-1} in
224 the Raman spectrum of parabutlerite.
225

The Raman spectra of butlerite and parabutlerite in the 100 to 800 cm^{-1} region are displayed in Figs. 3a and 3b, respectively. Ross [27] has reported the infrared bands of the ν_4 SO_4^{2-} bending modes at 595, 618 and 680 cm^{-1}. The Raman bands and/or shoulders for butlerite at 543, 600 and 617 cm^{-1} are ascribed to the $\nu_4 (SO_4)^{2-}$ bending modes. The observation of multiple bands suggests that the symmetry of the SO_4^{2-} tetrahedra has been reduced from T_d to a much lower symmetry C_{2v} or C_1. The Raman spectrum of parabutlerite shows bands and/or shoulders at 550, 614 and 655 cm^{-1}, which are also attributed to the ν_4 $(SO_4)^{2-}$ bending modes. However, some of these bands may be connected with the libration modes of water molecules. Ross [27], based upon the infrared spectrum of römerite, defined the $\nu_2 (SO_4)^{2-}$ bending modes at 460 and 494 cm^{-1}. Two Raman bands at 408 and 469 cm^{-1} and shoulders at 374 and 450 cm^{-1} are attributed to the $\nu_2 (SO_4)^{2-}$ bending modes, molecular water and hydroxyl ion libration modes in the butlerite spectrum. The spectrum of parabutlerite appears less complex for this spectral region with three Raman bands at 368, 406, and 468 cm^{-1} assigned to the $\nu_2 (SO_4)^{2-}$ bending modes and molecular water or hydroxyl ion libration modes. Bands observed at lower wavenumbers than 300 cm^{-1} (154, 181, 221, 247 and 294 cm^{-1} for butlerite, and 155, 186, 214, 237 and 263 cm^{-1} for parabutlerite) are assigned to the Fe-O and Fe-OH stretching vibrations and lattice vibrations [26].

The infrared spectra of butlerite and parabutlerite in the 700 to 400 cm^{-1} region are displayed in Figs. 4a and 4b. Strong infrared bands and shoulders are observed at 454, 492, 580, 594 and 657 cm^{-1} for butlerite and at 468, 503, 597, 621 and 657 cm^{-1} for parabutlerite. The latter three bands and shoulders for butlerite and parabutlerite are ascribed to the ν_4 $(SO_4)^{2-}$ bending modes. The observation of multiple bands suggests that the symmetry of the SO_4^{2-} tetrahedra has been reduced as was observed in the Raman spectrum. The two infrared bands and shoulders at 454 and 492 cm^{-1} for butlerite and at 468 and 503 cm-1 are attributed to the $\nu_2 (SO_4)^{2-}$ bending modes. The observation of multiple bands supports the concept of a reduction in symmetry of the sulfate anion.

The Raman spectra of butlerite and parabutlerite in the OH stretching region are reported in Figs. 5a and 5b, respectively. In the Raman spectrum of butlerite, bands are observed at 3310 and 3469 cm^{-1} with additional bands resolved at 3155 and 3012 cm^{-1}. The band at 3469 cm^{-1} is assigned to the ν OH stretching vibration of relatively weakly hydrogen bonded hydroxyl ions. The other three bands (3310, 3155 and 3012 cm^{-1}) are attributed to the

ν OH stretching vibrations of hydrogen bonded water molecules and hydroxyls. The Raman spectrum of parabutlerite is similar with Raman bands resolved at 3133, 3200, 3316 and 3504 cm^{-1}. Similarly, as in the case of butlerite, the band at 3504 cm^{-1} is assigned to the ν OH stretching vibrations of relatively weakly hydrogen bonded hydroxyls, while the remaining three bands (3316, 3200 and 3133 cm^{-1}) are assigned to the ν OH stretching vibrations of hydrogen bonded water molecules and hydroxyls. According to Libowitzky empirical equation [28], O-H...O hydrogen bond lengths vary in the range from 2.87 to 2.66 Å (butlerite) and from 2.90 to 2.69 Å (parabutlerite). These values are comparable with 2.86-2.60 Å for butlerite [6] and 2.93-2.61 Å [7], inferred from their X-ray single crystal structure analysis.

In contrast, the infrared spectra of butlerite and parabutlerite in the OH stretching region show a broad band with minimal features. The infrared spectra of butlerite and parabutlerite in the 3800 to 2300 cm^{-1} region are displayed in Figs. 6a and 6b. Infrared bands and shoulders are resolved at 2632, 2823, 3039, 3195, 3336 and 3476 cm^{-1} for butlerite and at 2814, 3021, 3177, 3335 and 3487 cm^{-1} for parabutlerite. The infrared shoulders at 3476 and 3487 cm^{-1} are connected with only weakly hydrogen-bonded hydroxyls, respectively. The other infrared bands and shoulders observed in this region are assigned to hydrogen-bonded water molecules and probably also hydroxyls in the case of both minerals studied. Inferred O-H...O hydrogen bond lengths [28] vary in the range 2.59-2.87 Å for butlerite and 2.62-2.88 Å for parabutlerite. This is also in agreement with X-ray single crystal structural analysis data for both minerals studied. The infrared spectra of butlerite and parabutlerite in the 1800 to 1300 cm^{-1} region are displayed in Figs. 7a and 7b. The spectra show strong asymmetry on the low wavenumber side. Infrared bands are observed at 1440, 1577, 1633 and 1644 cm^{-1} for butlerite and at 1502, 1615, 1651 and 1671 cm^{-1} for parabutlerite. The infrared bands at 1633 and 1664 cm^{-1} for butlerite and 1651 and 1671 cm^{-1} for parabutlerite are assigned to the water bending modes. The observation of bands in these positions provides evidence for water being strongly hydrogen bonded in the structure. The observation of two bands provides evidence for the non-equivalence of water in the butlerite and parabutlerite structure. The infrared bands at 1440 and 1577 cm^{-1} for butlerite and that at 1502 cm^{-1} for parabutlerite may probably be assigned to the overtones, combination bands or δ Fe-OH bending vibrations.

CONCLUSIONS

(1) Raman and infrared spectra of two polymorphous minerals monoclinic butlerite and orthorhombic parabutlerite, both having the same chemical formula $Fe^{3+}(SO_4)(OH)\cdot 2H_2O$, are recorded and interpreted.

(2) Observed Raman and infrared bands and shoulders are assigned to the $(SO_4)^{2-}$ stretching and bending vibrations, hydrogen bonded water molecules, hydroxyl ion stretching and bending vibrations, and libration modes of water molecules and hydroxyl ions. Low wavenumber bands are assigned to Fe-O and Fe-OH stretching vibrations, Fe-OH bending vibrations and lattice vibrations.

(3) O-H...O hydrogen bond lengths inferred from the Raman spectra 2.87 to 2.66 Å (butlerite) and 2.90 to 2.69 Å (parabutlerite) and from the infrared spectra 2.87 to 2.59 Å (butlerite) and 2.88 to 2.62 Å (parabutlerite) are comparable with ones calculated from the crystal structure refinement.

(4) Observed Raman and infrared bands and shoulders of butlerite and parabutlerite are similar but not identical. The presence of one symmetrically distinct $(SO_4)^{2-}$ unit in the structure of butlerite and two symmetrically distinct $(SO_4)^{2-}$ units in the structure of parabutlerite are distinctly expressed, especially from their Raman spectra.

Acknowledgements

The financial and infra-structure support of the Queensland University of Technology Chemistry Discipline of the Faculty of Science and Technology is gratefully acknowledged. The Australian Research Council (ARC) is thanked for funding the instrumentation. This work was financially supported by Ministry of Culture of the Czech Republic (MK00002327201) to Jiří Sejkora and Jakub Plášil.

Table 1 Factor group analysis

Butlerite
$Fe(SO_4)(OH)\cdot 2H_2O$ Z = 2

Number of fundamental modes = 3n - 3 = 81

SO_4

Td	Cs	C2h
A1	A'	Ag + Bu
E	A' + A"	Ag + Bu + Bg + Au
F2	2A' + A"	2Ag + 2Bu + Bg + Au
F2	2A' + A"	2Ag + 2Bu + Bg + Au

Parabutlerite
$Fe(SO_4)(OH)\cdot 2H_2O$ Z = 8

Number of fundamental modes = 3n - 3 = 333

2 x SO_4

Td	Cs	D2h
A1	A'	Ag + B3g + B1u + B2u
E	A' + A"	Ag + B3g + B1u + B2u + B1g + B2g + Au + B3u
F2	2A' + A"	2Ag + 2B3g + 2B1u + 2B2u + B1g + B2g + Au + B3u
F2	2A' + A"	2Ag + 2B3g + 2B1u + 2B2u + B1g + B2g + Au + B3u

329

330 **Table 2. Results of the Raman spectra of butlerite and parabutlerite (cm^{-1})**

331

butlerite	parabutlerite	assignment
3469	3504	ν OH stretch of $(OH)^-$ ions
3310, 3155, 3012	3316, 3200, 3133	ν OH stretch of H_2O and $(OH)^-$ ions
1225, 1198, 1145, 1109, 1088	1202, 1164, 1109, 1095	ν_3 $(SO_4)^{2-}$ antisymmetric stretch
1024	1044, 1026, 1014	ν_1 $(SO_4)^{2-}$ symmetric stretch
	990	Fe-OH bend
617, 600, 543	655, 614, 550	ν_4 $(SO_4)^{2-}$ antisymmetric bend
469, 450, 408, 374	468, 406, 368	ν_2 $(SO_4)^{2-}$ symmetric bend and water molecules and/or $(OH)^-$ libration modes
294, 247, 221, 181, 154	263, 237, 214, 186, 155	Fe-O and Fe-OH stretch and lattice vibrations

332

333

334 **Table 3. Results of the infrared spectra of butlerite and parabutlerite (cm^{-1})**

335

butlerite	parabutlerite	assignment
3476	3487	ν OH stretch of weakly hydrogen bonded$(OH)^-$ ions
3336, 3195, 3039	3335, 3177,3021	ν OH stretch of hydrogen bonded H_2O and $(OH)^-$ ions
2822, 2632	2814	ν OH stretch of hydrogen bonded H_2O and $(OH)^-$ ions
1664, 1633	1671, 1651, 1615	ν_2 (δ) H_2O bend
1577, 1440	1502	overtones(?), combination bands(?), δ Fe-OH bend(?)
1225, 1175, 1099, 1050	1228, 1173, 1131, 1097, 1051	ν_3 $(SO_4)^{2-}$ antisymmetric stretch
998	994	ν_1 $(SO_4)^{2-}$ symmetric stretch
950	956	δ Fe-OH bend
657, 594, 580	657, 621, 597	ν_4 $(SO_4)^{2-}$ bend
492, 454	468	ν_2 $(SO_4)^{2-}$ bend

336
337
338
339
340

References

[1] Majzlan, J., Navrotsky, A., McCleskey, B., Alpers, C.N., Eur. J. Mineral. 182 (2006), 175-186.

[2] Klingelhöfer G, Morris RV, Bernhardt B, Schröder C, Rodinov DS, De Souza PA, Yen A, Gellert R, Evlanov EN, Zubkov B, Foh J, Bonnes U, Kankeleit E, Gütlich P, Ming DW, Renz F, Wdowiak t, Squyres SW, Arvidson RE, Science 306 (2004), 1740-1745 .

[3] T. Buckby, S. Black, M.L. Coleman, M.E. Hodson, Mineral. Mag. 67 (2003) 263-278.

[4] P. A. Williams, Oxide Zone Geochemistry, Ellis Horwood Ltd, Chichester, West Sussex, England, 1990.

[5] F. Cesbron, Bull. Soc. Franç. Minér. Crist. 87 (1964) 125-143.

[6] L. Fanfani, A. Nunzi, P. F. Zanazzi, Am. Mineral. 56 (1971) 751-757.

[7] J. Borène, Bull. Soc. Franç. Minéral. Crist. 93 (1970) 185-189.

[8] J. W. Anthony, R. A. Bideaux, R. W. Bladh, M. C. Nichols, Handbook of Mineralogy, Vol. V, Borates, Carbonates, Sulfates. Mineral Data Publishing, Tucson, Arizona 2003.

[9] C. Sabelli, R. Trosti-Ferroni, Periodico Mineral. 54 (1985) 1-46.

[10] D. Yu. Pushcharovsky, J. Lima-de-Faria, R. K. Rastsvetaeva, Z. Kristallogr. 213 (1998) 141-150.

[11] L. F. Aristarian, Rev. Mus. Argentina Cienc. Nat., n. s. 1 (2) (1999) 145-150.

[12] D. A. Cole, G. W. Simmons, R. G. Herman, K. Klier, I. Czako-Nagy, Fuel 66 (1987) 1240-1248.

[13] M. C. Brandy, Am. Mineral. 23 (1938) 669-760.

[14] F.C. Hawthorne, Acta Crystallogr. B50 (1994) 481-510.

[15] F. C. Hawthorne, EMU Notes in Mineralogy 1 (1997) 373-429.

[16] F. C. Hawthorne, S. V. Krivovichev, P. C. Burns, Rev. Mineral. Geochem. 40 (2000) 1-112.

[17] M Schindler, D.M.C. Huminicki, F.C. Hawthorne, Can. Mineral. 44 (2006) 1403-1429.

[18] F. Scordari, Tschermaks Mineral. Petrogr. Mitt. 28 (1981) 17-29.

[19] J. Sejkora, J. Škovíra, J. Čejka, J. Plášil, J. Geosci. 54 (2009), 355-371.

376 [20] J. Sejkora, D. Ozdín, R. Ďuďa, J. Geosci. 55 (2010), 149-160.
377 [21] R. L. Frost, S. Bahfenne, J. Čejka, J. Sejkora, J. Plášil, S. J. Palmer, J. Raman
378 Spectrosc. 41 (2010), 814-819.
379 [22] R. L. Frost, S. Bahfenne, J. Čejka, J. Sejkora, S. J. Palmer, R. Škoda, J. Raman
380 Spectrosc. 41 (2010), 690-693.
381 [23] S.C.B. Myneni, Rev. Mineral. Geoch. 40 (2000) 113-172.
382 [24] K. Nakamoto, Infrared and Raman Spectra of Inorganic and Coordination Compounds.
383 John Wiley & Sons, New York 1986.
384 [25] V.C. Farmer (Ed.), The infrared spectra of minerals, The Mineralogical Society, London
385 1974.
386 [26] H.D. Lutz, Structure Bond. 82 (1995) 85-103.
387 [27] S.D. Ross in The Infrared Spectra of Minerals (V.C. Farmer, Ed.), p. 423-444. The
388 Mineralogical Society London 1974.
389 [28] E. Libowitzky, Monatsh. Chem. 130 (1999) 1047-1059.
390

391 **List of Figures**

392

393 **Fig. 1. Raman spectra of (a) butlerite and (b) parabutlerite in the 1300 to**
394 **900 cm^{-1} region.**

395

396 **Fig. 2. Infrared spectra of (a) butlerite and (b) parabutlerite in the 1300 to**
397 **700 cm^{-1} region.**

398

399 **Fig. 3. Raman spectra of (a) butlerite and (b) parabutlerite in the 800 to**
400 **100 cm^{-1} region.**

401

402 **Fig. 4. Infrared spectra of (a) butlerite and (b) parabutlerite in the 700 to**
403 **400 cm^{-1} region.**

404

405 **Fig. 5. Raman spectra of (a) butlerite and (b) parabutlerite in the 3800 to**
406 **2600 cm^{-1} region.**

407

408 **Fig. 6. Infrared spectra of (a) butlerite and (b) parabutlerite in the 3800 to**
409 **2300 cm^{-1} region.**

410

411 **Fig. 7. Infrared spectra of (a) butlerite and (b) parabutlerite in the 1800 to**
412 **1300 cm^{-1} region.**

413

414

415

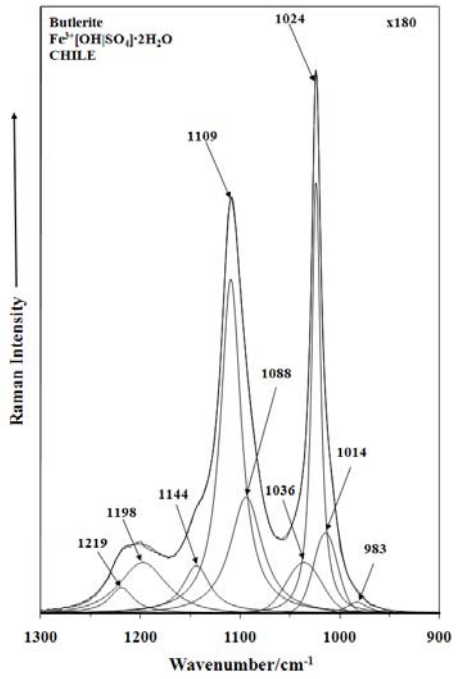

Figure 1a Raman spectrum of butlerite in the 1300 to 900 cm^{-1} region.

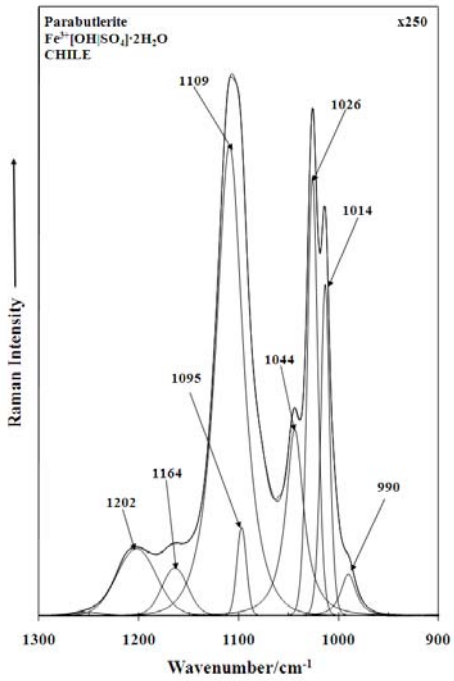

Figure 1b Raman spectrum of parabutlerite in the 1300 to 900 cm^{-1} region.

416

417

418

419

420

421

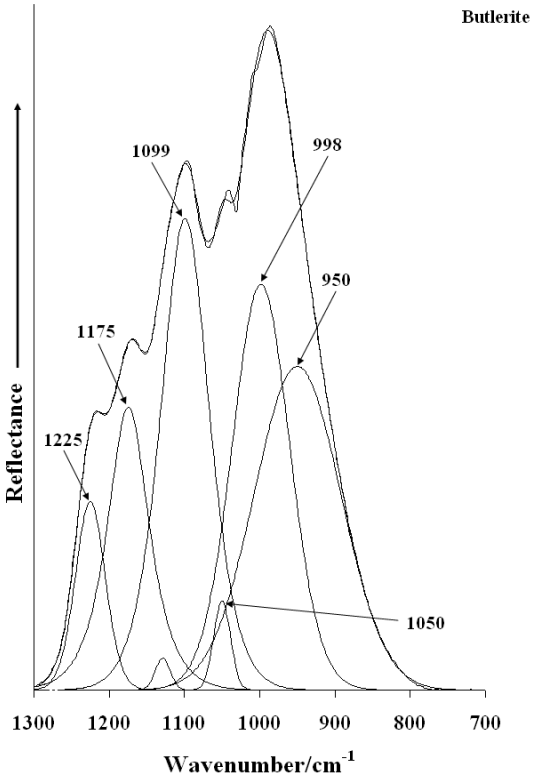

Figure 2a Infrared spectrum of butlerite in the 1300 to 700 cm^{-1} region.

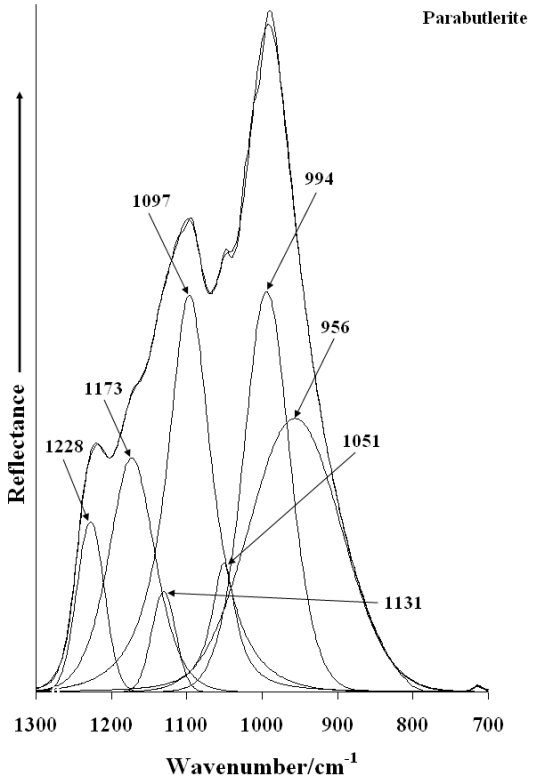

Figure 2b Infrared spectrum of parabutlerite in the 1300 to 700 cm^{-1} region.

422

423

424

425

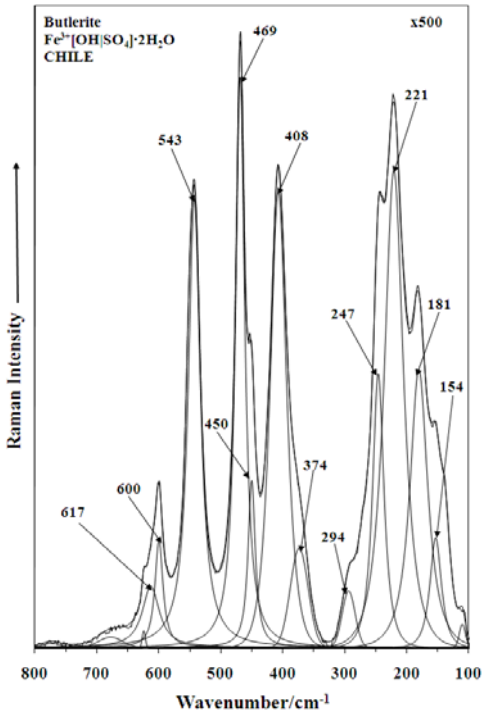

Figure 3a Raman spectrum of butlerite in the 800 to 100 cm^{-1} region.

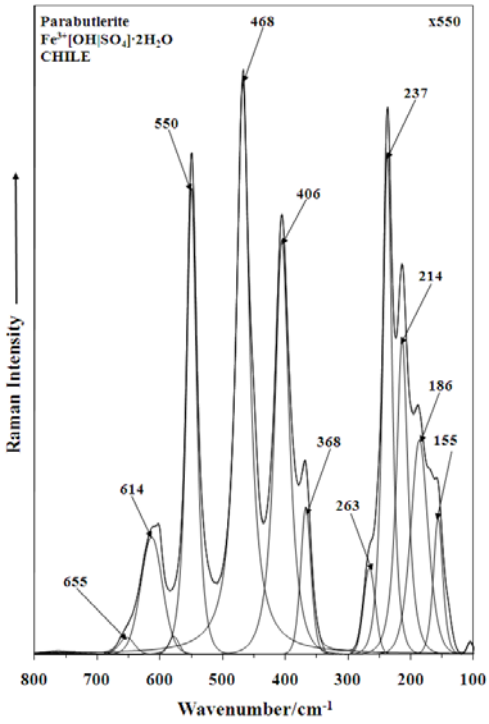

Figure 3b Raman spectrum of parabutlerite in the 800 to 100 cm^{-1} region.

426

427

428

429

430

431

432

433

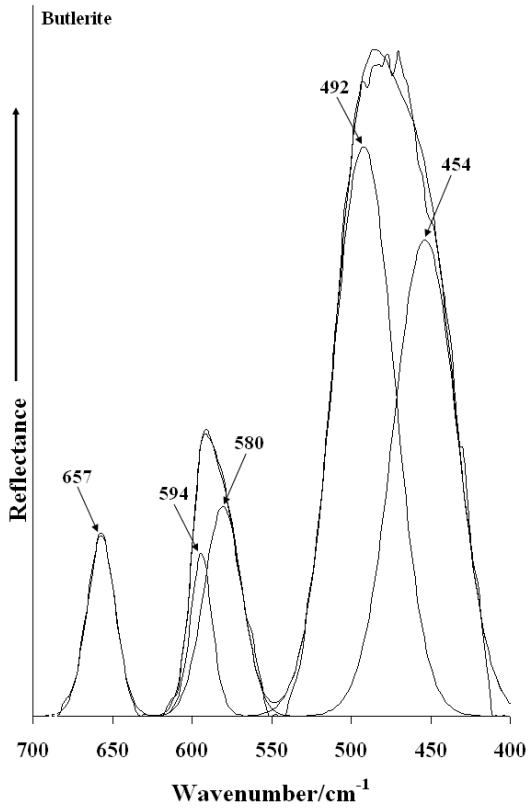

Figure 4a Infrared spectrum of butlerite in the 700 to 400 cm^{-1} region.

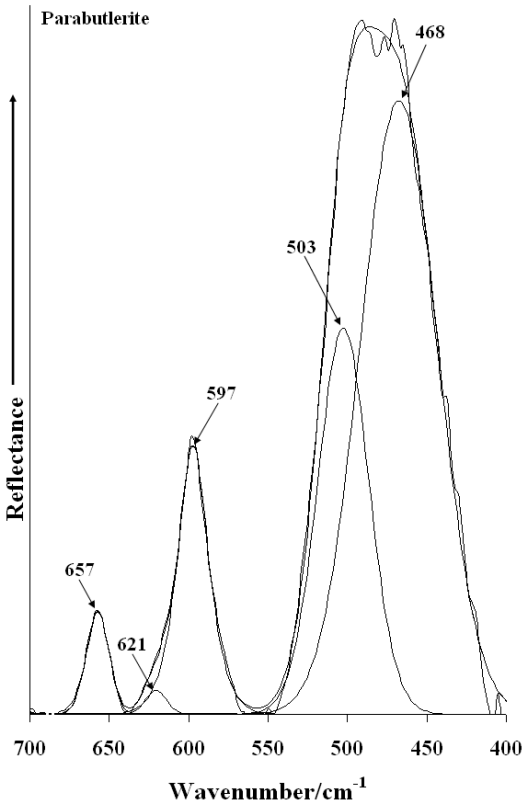

Figure 4b Infrared spectrum of parabutlerite in the 700 to 400 cm^{-1} region.

434

435

436

437

438

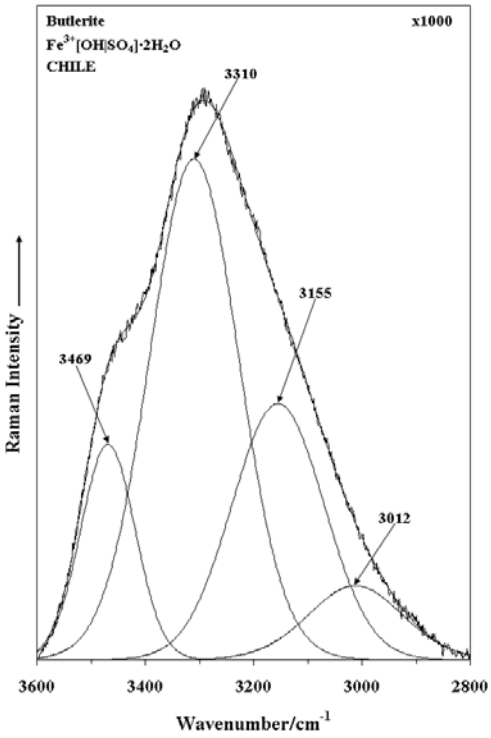

Figure 5a Raman spectrum of butlerite in the 3600 to 2800 cm^{-1} region.

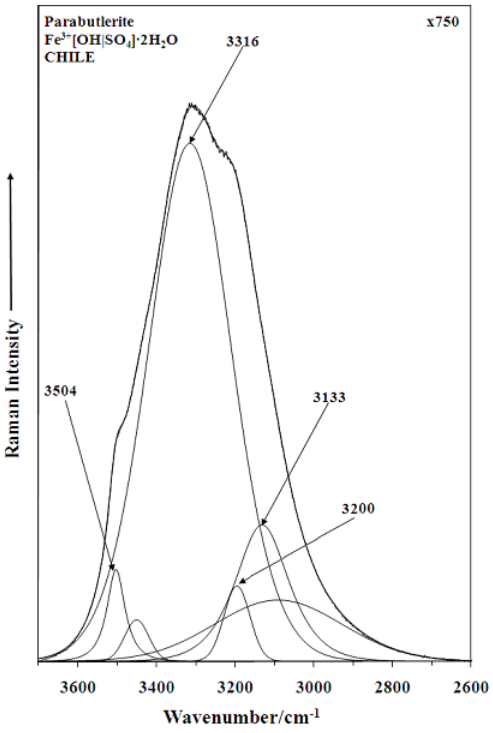

Figure 5b Raman spectrum of parabutlerite in the 3700 to 2600 cm^{-1} region.

439

440

441

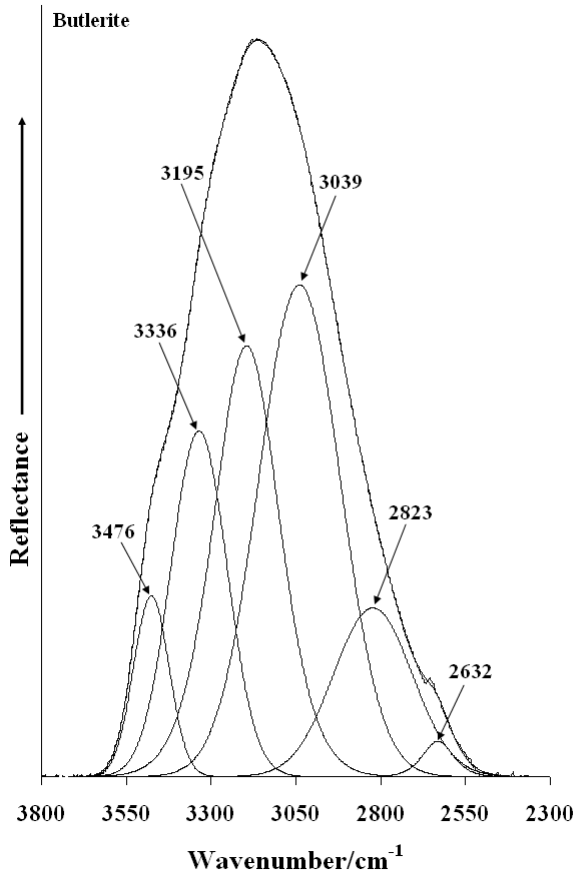

Figure 6a Infrared spectrum of butlerite in the 2300 to 3800 cm^{-1} region.

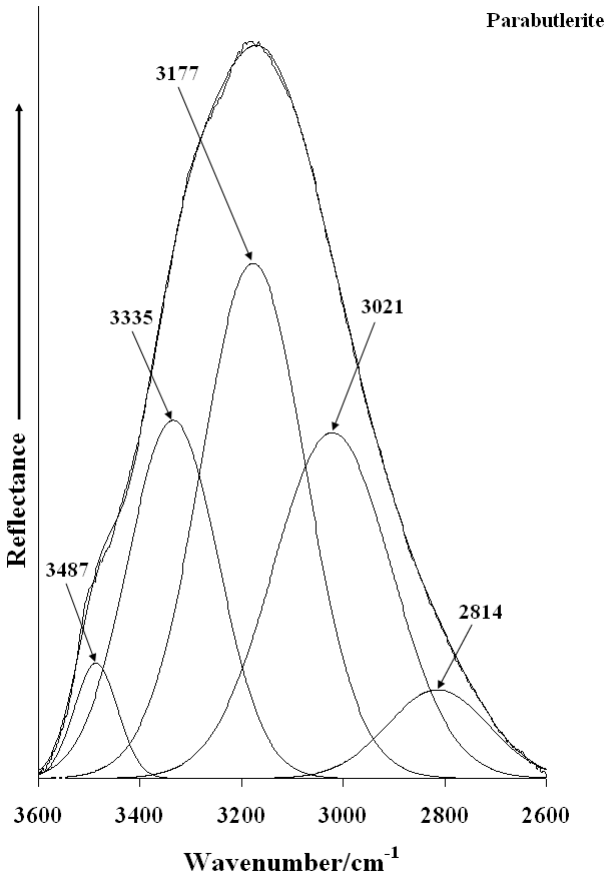

Figure 6b Infrared spectrum of parabutlerite 2600 to 3800 cm^{-1} region.

442

443

444

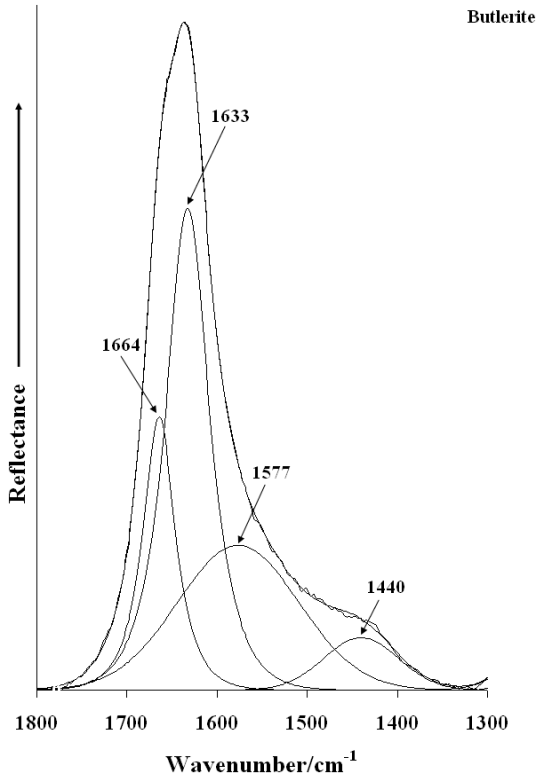

Figure 7a Infrared spectrum of butlerite in the 1300 to 1800 cm^{-1} region.

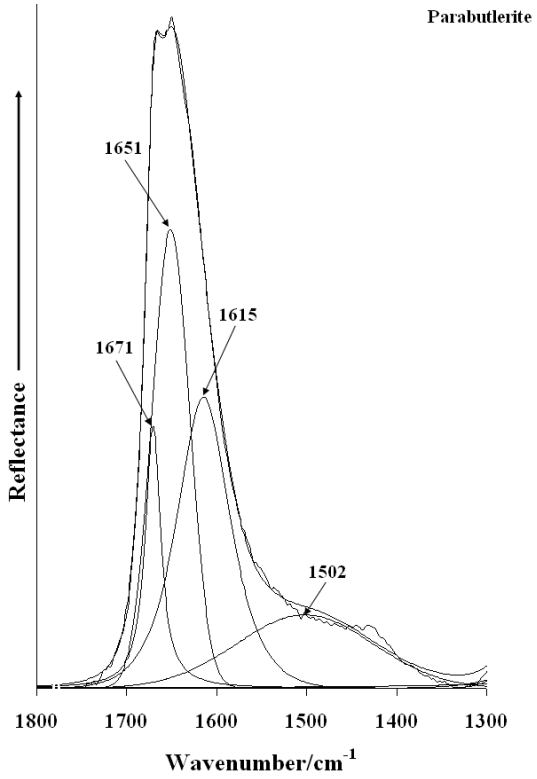

Figure 7b Infrared spectrum of parabutlerite 1300 to 1800 cm^{-1} region.

445